

Dynamical renormalization of electron-phonon coupling in conventional superconductors

Nina Girotto¹ and Dino Novko^{1,*}

¹*Institute of Physics, 10000 Zagreb, Croatia*

The adiabatic Born-Oppenheimer approximation is considered to be a robust approach that very rarely breaks down. Consequently, it is predominantly utilized to address various electron-phonon properties in condensed matter physics. By combining many-body perturbation and density functional theories we demonstrate the importance of dynamical (nonadiabatic) effects in estimating superconducting properties in various bulk and two-dimensional materials. Apart from the expected long-wavelength nonadiabatic effects, we found sizable nonadiabatic Kohn anomalies away from the Brillouin zone center for materials with strong intervalley electron-phonon scatterings. Compared to the adiabatic result, these dynamical phonon anomalies can significantly modify electron-phonon coupling strength λ and superconducting transition temperature T_c . Further, the dynamically-induced modifications of λ have a strong impact on transport properties, where probably the most interesting is the rescaling of the low-temperature and low-frequency regime of the scattering time $1/\tau$ from about T^3 to about T^2 , resembling the Fermi liquid result for electron-electron scattering. Our goal is to point out the potential implications of these nonadiabatic effects and reestablish their pivotal role in computational estimations of electron-phonon properties.

INTRODUCTION

Electron-phonon coupling (EPC) is crucial for understanding a vast number of phenomena in condensed matter physics, including resistivity, optical absorption, band gap renormalizations, structural phase transitions, charge density waves, and superconductivity [1]. Most of the theoretical considerations of these properties rely on the adiabatic Born-Oppenheimer approximation, where electron and lattice degrees of freedom are treated separately and the dynamical effects of EPC are absent [2]. However, there are certain conditions under which the adiabatic approximation fails. Specifically, provided that the electronic dampings are negligible, optical phonons around the center of the Brillouin zone (i.e., $\mathbf{q} \cdot \mathbf{v}_F < \omega$ and $1/\tau \ll \omega$) are expected to be affected by the nonadiabatic (NA) corrections [3–5]. The latter was confirmed by various theoretical and experimental (e.g., Raman and inelastic x-ray scattering) works, where profound NA renormalizations of optical phonons were found, for instance, in doped bulk semiconductors [6], MgB_2 [7–11], transition metals [12, 13], graphene-based materials [14–17], hole-doped diamond [18], and doped transition metal dichalcogenides [19–21].

Besides these studies, where the focus is on long-wavelength optical phonons and several others where NA effects and electron band structure renormalizations are analyzed [22, 23], there are very few quantitative studies going beyond and exploring self-consistently dynamical corrections of electron-phonon properties in realistic materials, like the coupling strengths, superconductivity, and resistivity [24, 25]. Namely, it was shown that the dynamical screening of phonons, provided by the combination of molecular dynamics and real-time time-

dependent-density-functional theory, can lead to significant modifications of EPC strength λ and superconductivity transition temperature T_c [24], as well as, potential energy surfaces and anharmonicity [25]. In addition, important insights were provided by the model calculations (e.g., Holstein Hamiltonian), where the influence of the dynamical phonon renormalization [26–30] and vertex corrections [31–33] on superconductivity was demonstrated. For example, it was shown that replacing the bare (adiabatic) phonon propagator with the renormalized one (i.e., including phonon self-energy corrections) in Migdal-Eliashberg equations improves considerably its accuracy [27, 28]. Also, accounting for phonon self-energy corrections, damping in particular, was found to be instrumental for describing the superconducting dome structure in ferroelectric materials [30].

Notwithstanding, the majority of the theoretical first-principles studies of superconductivity are done in the framework of the adiabatic approximation [1], and the role of NA corrections is still not fully established.

Here we provide a detailed *ab initio* study on the NA phonon renormalizations and the corresponding impact on λ , T_c , as well as electron scattering rates $1/\tau$ relevant in transport and optical absorption. We use density functional perturbation theory (DFPT) [2] and NA phonon self-energies [1, 34] in order to simulate NA corrections to phonon frequencies and linewidths, which in turn are utilized to renormalize electron-phonon properties. We investigate the NA effects in several relevant bulk and two-dimensional (2D) systems, where conventional, phonon-mediated superconductivity was confirmed by both experiments and theory or just in theory, i.e., MgB_2 [35–43], hole-doped diamond (C) [44–48], and doped monolayers: graphene (1L Gr) [49–51], graphane (1L Gr-H) [52], molybdenum disulfide (1L MoS_2) [53–59], arsenene (1L As) [60], indium selenide (1L InSe) [61, 62], and wolfram ditelluride (1L WTe_2) [63, 64]. Contrary to the common belief, our results show that the NA

* dino.novko@gmail.com

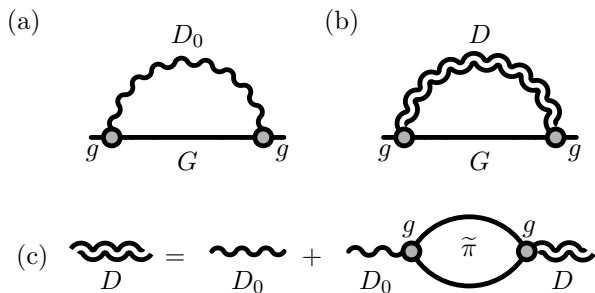


FIG. 1. (a) Diagrammatic representation of the electron self-energy $\Sigma = g^2GD_0$, where g are the screened EPC matrix elements (grey circles), G is the electron Green's function (straight line) and D_0 is the bare phonon propagator (single wavy line). (b) The electron self-energy $\Sigma = g^2GD$, where the bare phonon propagator D_0 is replaced with the dynamical (NA) phonon propagator D (double wavy line). (c) Dressing of the phonons via the dynamical EPC, i.e., the Dyson equation for the phonon propagator $D = D_0 + D_0\tilde{\pi}D$, where $\tilde{\pi}$ is the NA phonon self-energy due to EPC.

frequency renormalization can be significant also away from the long-wavelength $\mathbf{q} \approx 0$ region, especially in the multiband and multivalley systems such as MgB_2 , MoS_2 , As, and WTe_2 , where strong interband or intervalley electron-phonon scatterings are possible, forming Kohn anomalies. Further, compared to the adiabatic calculations, we obtained considerable modifications of λ and T_c once the NA phonon frequency renormalizations and phonon linewidths due to EPC are taken into account. Specifically, the relative changes of λ , when going from adiabatic to NA results, can range from small (e.g., 3% for MgB_2) to considerable (e.g., 42% for 1L InSe). The obtained modifications for T_c are even more dramatic, varying from 10% in the case of MgB_2 to about 80% for 1L MoS_2 and 1L InSe. Interestingly, in most cases, the NA effects lead to the reduction of λ , while for MgB_2 and C the inclusion of the dynamical phonon linewidths into the calculations of EPC results its increase. Finally, we show how the dynamical electron-phonon effects can significantly influence, both qualitatively and quantitatively, the functional dependence of the electron-hole pair scattering rate $1/\tau_{\text{op}}(\omega, T)$ and mass enhancement factor $\lambda_{\text{op}}(\omega, T)$ [65, 66] on frequency ω and temperature T . For instance, the inclusion of the NA effects modifies the well-known behaviour of $1/\tau_{\text{op}} \propto T^3$ to $1/\tau_{\text{op}} \propto T^2$ [26, 67], resembling the Fermi liquid result for electron-electron scatterings. The latter might provide further insights into enigmatic T^2 resistivity observed in a number of complex materials [68–74].

RESULTS

A central quantity in many-body perturbation theory for describing electron dynamics due to EPC is the electron self-energy Σ , which is instrumental for understand-

ing quasiparticle spectral features [75, 76], superconductivity properties, such as T_c [66, 77], electron scattering rates, and electron resistivity [26]. Schematically, the electron self-energy can be written as $\Sigma = g^2GD$, where g are the screened EPC matrix elements, G is the electron Green's function and D is the phonon propagator [see diagram in Fig. 1(a)]. In the standard calculations of Σ based, e.g., on DFPT, the phonon propagator D is non-interacting with sharp (i.e., having infinite lifetime) adiabatic phonons [1, 2, 34]. In the following we inspect how general electron-phonon properties are modified when dynamical properties are accounted for in D via NA EPC, as diagrammatically depicted in Figs. 1(b) and 1(c), where additional interaction between phonons and electron-hole pairs brings about finite phonon lifetime and frequency renormalizations.

When averaged over the Fermi surface, the electron self-energy Σ is commonly expressed via the electron-phonon spectral function or the Eliashberg function [26, 77]

$$\alpha^2F(\omega) = \frac{1}{\pi N(E_F)} \sum_{\mathbf{q}\nu} \frac{\gamma_{\mathbf{q}\nu}}{\Omega_{\mathbf{q}\nu}} B_\nu(\mathbf{q}, \omega), \quad (1)$$

where \mathbf{q} and ν are phonon momentum and branch index, $N(E_F)$ is the density of states at the Fermi level, $\gamma_{\mathbf{q}\nu}$ are the phonon linewidths in the double-delta approximation [78], $\Omega_{\mathbf{q}\nu}$ are the phonon frequencies, while $B_\nu(\mathbf{q}, \omega)$ is the phonon spectral function. If one accounts for the dynamical EPC effects, the latter quantities can be expressed via the NA phonon self-energy $\tilde{\pi}_\nu(\mathbf{q}, \omega)$, i.e., $\gamma_{\mathbf{q}\nu} = -\text{Im} \tilde{\pi}_\nu(\mathbf{q}, \Omega_{\mathbf{q}\nu})$, $\Omega_{\mathbf{q}\nu}^2 = \omega_{\mathbf{q}\nu}^2 + 2\omega_{\mathbf{q}\nu} \text{Re} \tilde{\pi}_\nu(\mathbf{q}, \Omega_{\mathbf{q}\nu})$,

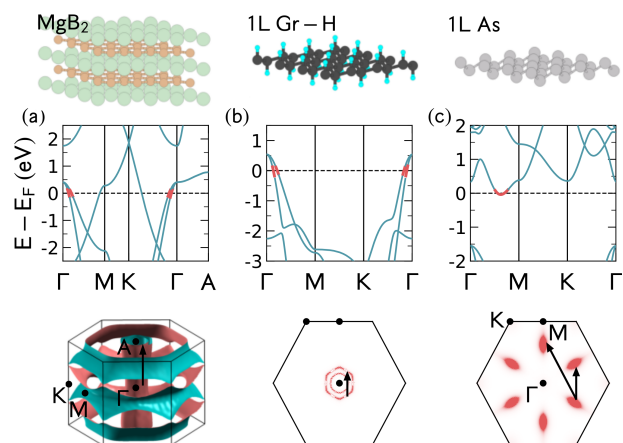


FIG. 2. Structure, electronic bands along high-symmetry points of the Brillouin zone, and Fermi surface in the first Brillouin zone for (a) MgB_2 , (b) graphane (1L Gr-H), and (c) arsenene (1L As). Red color highlights the relevant electronic states at the Fermi level that are involved in electron-phonon scatterings and formation of the (adiabatic and dynamical) Kohn anomalies. Black arrows depict the corresponding electronic transitions.

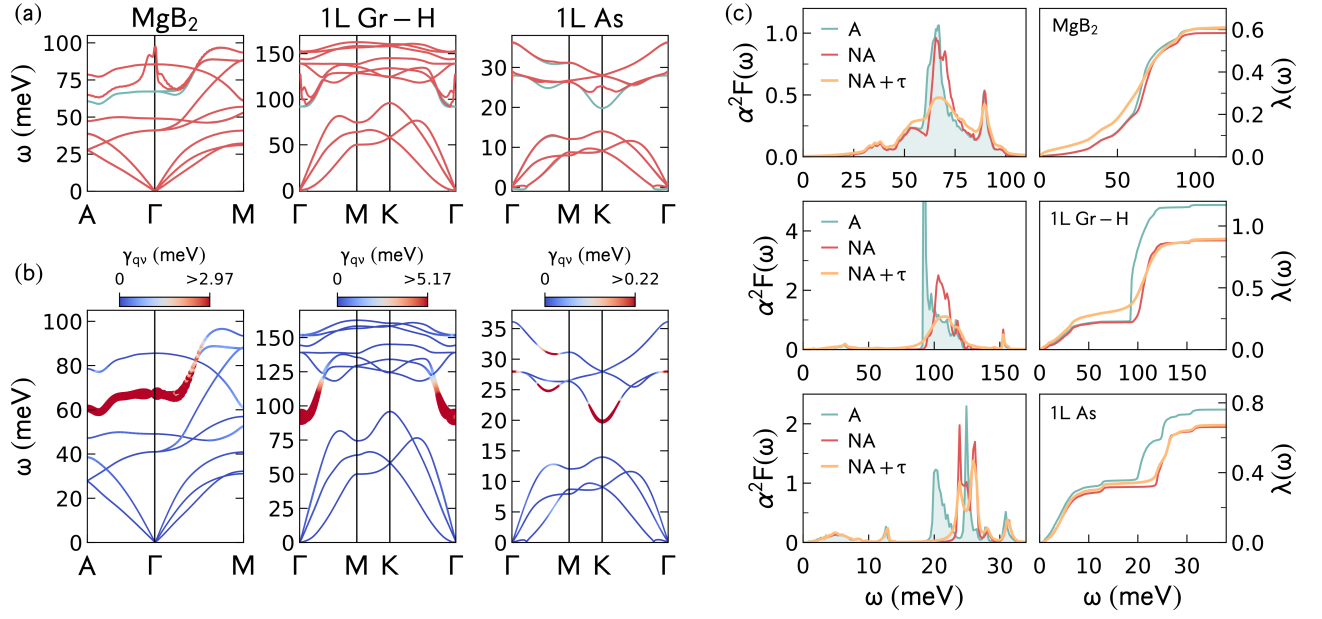


FIG. 3. (a) Adiabatic (A; blue) and nonadiabatic (NA; red) phonon dispersions of MgB_2 , monolayer graphane (1L Gr-H), and monolayer arsenene (1L As). Notice how strong dynamical corrections to the phonon bands can occur away from the center of the Brillouin zone, as it is the case in MgB_2 and 1L As. (b) The corresponding phonon linewidths $\gamma_{\mathbf{q}\nu}$ coming from the EPC. The size of the dots and colors (defined within the colorbars) represents the intensity of $\gamma_{\mathbf{q}\nu}$. (c) Eliashberg functions $\alpha^2 F(\omega)$ and cumulative EPC constant $\lambda(\omega)$ obtained for MgB_2 , 1L Gr-H, and 1L As. Three different results are shown: adiabatic (A), where frequencies are obtained within the adiabatic DFPT and without momentum and branch-resolved phonon broadenings $\gamma_{\mathbf{q}\nu}$ (blue), nonadiabatic (NA), where frequencies are corrected with NA effects, while the corresponding NA phonon broadening due to EPC is not included (red), and full nonadiabatic (NA+ τ), where both NA frequency renormalization and NA phonon linewidth effects are taken into account (yellow).

and

$$B_\nu(\mathbf{q}, \omega) = -\frac{1}{\pi} \text{Im} \left[\frac{2\omega_{\mathbf{q}\nu}}{\omega^2 - \omega_{\mathbf{q}\nu}^2 - 2\omega_{\mathbf{q}\nu} \tilde{\pi}_\nu(\mathbf{q}, \omega)} \right]. \quad (2)$$

Note that in the standard adiabatic simulations of the EPC properties, the dynamical effects are absent, and one calculates Eqs. (1) and (2) with $\tilde{\pi}_\nu(\mathbf{q}, \omega) \rightarrow i0$ [1, 34]. Here we calculate NA phonon self-energy as $\tilde{\pi}_\nu(\mathbf{q}, \omega) = \pi_\nu(\mathbf{q}, \omega) - \pi_\nu(\mathbf{q}, 0)$ [since the adiabatic frequency $\omega_{\mathbf{q}\nu}$ already contains $\pi_\nu(\mathbf{q}, 0)$], where

$$\pi_\nu(\mathbf{q}, \omega) = \sum_{\mathbf{k}n\mathbf{m}} |g_\nu^{nm}(\mathbf{k}, \mathbf{q})|^2 \frac{f_{n\mathbf{k}} - f_{m\mathbf{k}+\mathbf{q}}}{\omega + \varepsilon_{n\mathbf{k}} - \varepsilon_{m\mathbf{k}+\mathbf{q}} + i\eta}. \quad (3)$$

The electron-phonon matrix elements are denoted with $g_\nu^{nm}(\mathbf{k}, \mathbf{q})$, Fermi-Dirac distribution functions are $f_{n\mathbf{k}}$, $\varepsilon_{n\mathbf{k}}$ are electron energies, and η is an infinitesimal parameter. Equations (1)-(3) and the corresponding input parameters are calculated in this work by means of DFPT [2, 79] and Wannier interpolation [80] of EPC matrix elements g_ν^{nm} [34]. All the necessary computational details can be found in the Methods section and in the Supplementary Note 1.

In Fig. 2 we show the electronic structures of MgB_2 , hole-doped 1L Gr-H, and electron-doped 1L As. The electronic band structure of MgB_2 around the Fermi level consists of the hole-like σ states around the center, and

π states at the edges of the Brillouin zone. The former (red thicker lines) are the most relevant for the formation of the Kohn anomalies in the phonon spectra and provide a dominating contribution to the superconducting state. In 1L Gr-H the Fermi surface consists only of the hole σ states around the Γ point, while in 1L As there are 6 electron pockets appearing between the Γ and M points. All these states are involved in the strong electron-phonon scatterings (see arrows in Fig. 1), in these cases mostly with optical phonons, and are therefore an important contribution to the total electron-phonon coupling strength λ and superconducting properties. Band structures of other systems considered in this work (C, 1L Gr, 1L MoS_2 , 1L InSe, and 1L WTe_2) are provided in Supplementary Figure 1.

Calculations of the phonon dispersions and EPC strengths are outlined in Fig. 3, where standard adiabatic and dynamical results are compared. Interestingly, along with the expected NA frequency renormalizations at the Γ point for the systems with the strong EPC (1L Gr-H), there are considerable NA corrections of phonons away from the center of the Brillouin zone for MgB_2 and 1L As. As shown in Supplementary Figure 2, 1L MoS_2 , 1L InSe, and 1L WTe_2 are also characterized with strong dynamical Kohn anomalies away from the Γ point. Therefore, the NA condition $\mathbf{q} \cdot \mathbf{v}_\mathbf{F} < \omega$ [4, 5] only holds for simple metals with parabolic band structure, while

for the multiband systems, strong electron-phonon scatterings between same or different valleys could lead to NA Kohn anomalies at finite $\mathbf{q} = \mathbf{q}_c$, provided that the $\varepsilon_{n\mathbf{k}} - \varepsilon_{m\mathbf{k}+\mathbf{q}_c} \lesssim \omega$ condition is met. These $\mathbf{q} = \mathbf{q}_c$ dynamical transitions are shown with arrows in Fig. 2 for MgB_2 , 1L Gr-H, and 1L As, and represent the largest contributions to the electron-phonon scatterings and total EPC strength λ . For instance, in the case of MgB_2 strong NA corrections are present for the optical E_{2g} mode around the Γ point, but also extending along the $\Gamma - \text{M}$ line, exactly where the phonon linewidths $\gamma_{\mathbf{q}\nu}$ are largest. It is similar in other cases, where intra- (C, 1L Gr-H, 1L Gr, 1L InSe) and inter-valley (1L As, 1L MoS_2 , 1L WTe_2) electron-phonon scatterings bring about, at the same wavevector \mathbf{q}_c and phonon branch, strong NA corrections to phonon frequencies and large NA phonon linewidths $\gamma_{\mathbf{q}\nu}$.

The aforementioned two NA effects are often inseparable and should be included together when calculating the Eliashberg function $\alpha^2F(\omega)$ and the total EPC

strength λ . In Fig. 3(c) we show the results of $\alpha^2F(\omega)$ and cumulative EPC constant $\lambda(\omega) = 2 \int_0^\omega d\Omega \alpha^2F(\Omega)/\Omega$ for three different approaches. Namely, we use the standard adiabatic approximation, where no dynamical effects are considered in Eq. 1, i.e., $\tilde{\pi}_\nu(\mathbf{q}, \omega) \rightarrow i0$, (blue), the NA approach with only dynamical frequency renormalizations included, i.e., $\tilde{\pi}_\nu(\mathbf{q}, \omega) \rightarrow \text{Re}\tilde{\pi}_\nu(\mathbf{q}, \omega) + i0$, (red), and the full NA method with both frequency corrections and phonon dampings (yellow). The NA frequency renormalizations are always positive [1], and since these shifts are accompanied by strong phonon damping rates, the main peaks in $\alpha^2F(\omega)$ are blueshifted and λ is reduced. For example, the NA blueshifts of the Kohn anomalies of about 33 meV and 6 meV in 1L Gr-H and 1L As, respectively, is reflected in the corresponding modifications in $\alpha^2F(\omega)$ and in a considerable reduction of λ of about 0.29 and 0.14. By including additionally the momentum- and mode-resolved broadening $\gamma_{\mathbf{q}\nu}$, the total EPC constant λ is not affected seriously, however, the spectral weight of $\alpha^2F(\omega)$ is redistributed and smoothed, so that the high-frequency main peaks contribute less, while lower frequencies contribute more to $\lambda(\omega)$. This frequency redistribution of the EPC due to NA effects has pertinent consequences on the low-temperature and low-energy behavior of electron-hole scattering rate [26], as we will show below. For more data on $\alpha^2F(\omega)$ see Supplementary Figure 3.

Collected results for all of the studied systems is presented in Fig. 4, including the dynamical corrections of the total EPC strength λ , the first moment of the phonon spectrum $\lambda\langle\omega\rangle$, and the superconducting transition temperature T_c . The first moment is calculated as $\lambda\langle\omega\rangle = 2 \int_0^\infty d\Omega \alpha^2F(\Omega)$, and it is considered important for the McMillan's expression for T_c [81], as well as high-energy and zero-temperature estimation of the electron-hole relaxation rate $1/\tau_{\text{op}}$ appearing in the optical conductivity formula [65, 66, 82, 83]. For calculations of T_c we use Allen-Dynes version of McMillan's formula [84]. While in some cases the dynamical renormalizations of frequencies induce small relative modifications (compared to adiabatic result) of λ (MgB_2 , C), there are cases where it is significantly decreased, i.e., by 19% to 42% (MoS_2 , 1L InSe, 1L WTe_2 , and 1L Gr-H). This is reflected in mild and considerable reduction in T_c , respectively. For example, 8-12% for MgB_2 and 70-85% for InSe (as obtained with reasonable choices of effective Coulomb repulsion μ^*). In most cases the dynamical effects on $\lambda\langle\omega\rangle$ are small (largest being for 1L Gr-H), suggesting that high-energy limits of $1/\tau_{\text{op}}$ and, consequently, phonon-assisted optical absorption formula are not strongly affected by the NA renormalizations. Interestingly, the value of λ can be additionally increased by the NA phonon broadening effects, while T_c can be either increased or decreased, depending on an interplay between modifications in the position of strong peaks in $\alpha^2F(\omega)$ (via $\langle\omega\rangle$ or ω_{log}) and changes in λ . For instance, the phonon-broadening-induced reduction in ω_{log} (see Supplementary Figure 4) and increase in λ results in further decrease of T_c for

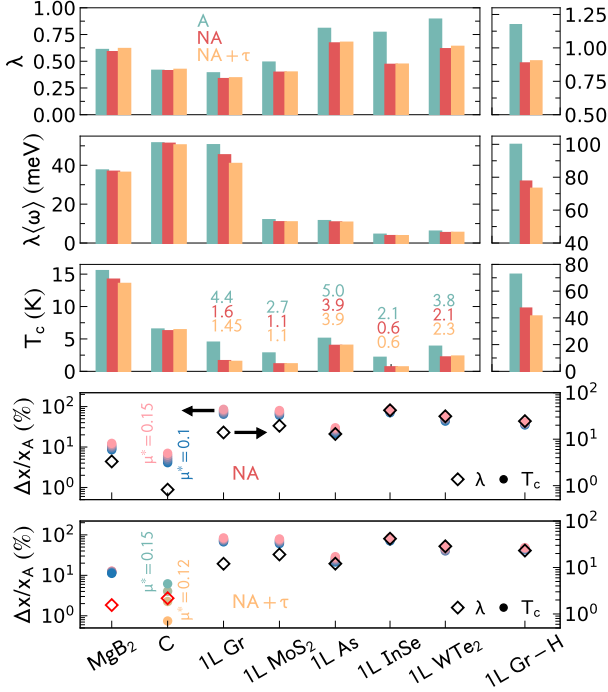


FIG. 4. The total EPC strengths λ , the first moments of the phonon spectrum $\lambda\langle\omega\rangle$, and superconducting transition temperatures T_c obtained with three different approaches: adiabatic (A; within standard adiabatic DFPT methodology), nonadiabatic (NA; by including NA phonon frequency renormalizations), and full nonadiabatic (NA+ τ ; by including both NA frequency renormalizations and NA phonon broadenings $\gamma_{\mathbf{q}\nu}$). The results are presented for various bulk and 2D superconducting materials. Bottom panels show the corresponding relative changes $(x_{\text{NA}/\text{NA}+\tau} - x_{\text{A}})/x_{\text{A}}$ for T_c (left axis) and λ (right axis). All relative changes are positive, except the NA+ τ results of $x = \lambda$ for MgB_2 and C (red diamond signs), and of $x = T_c$ for C (green-yellow circles).

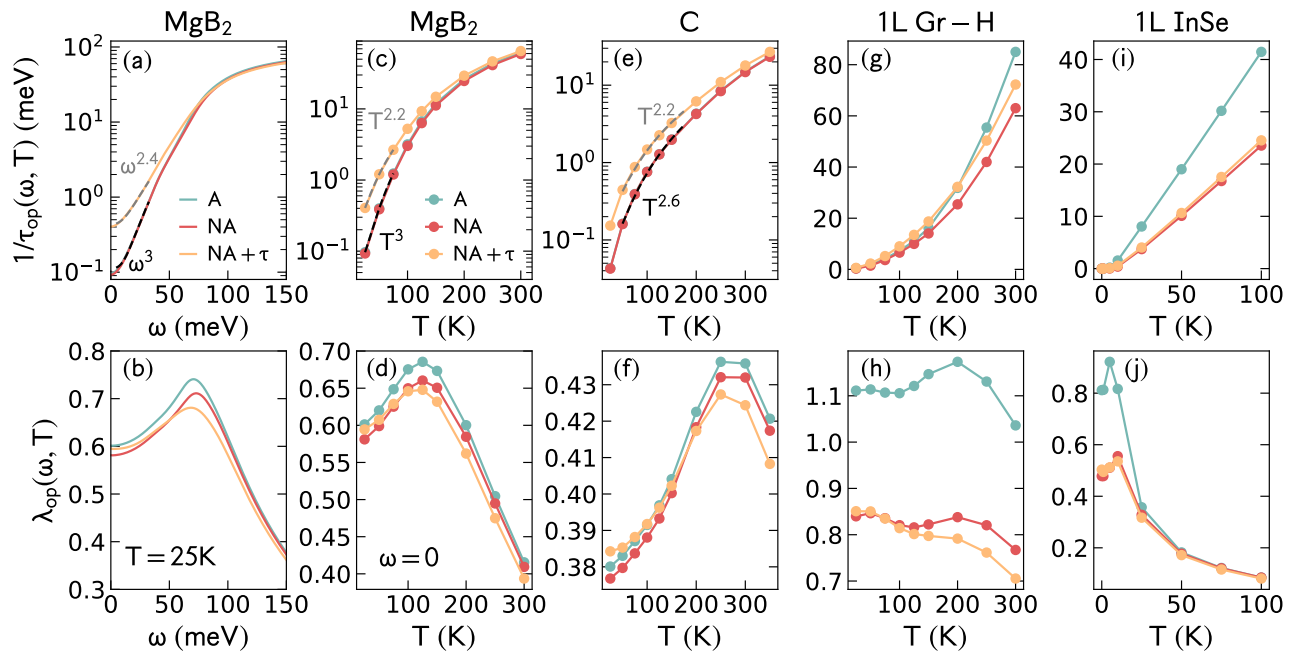


FIG. 5. Frequency and temperature dependence of the optical (or electron-hole pair) scattering rate $1/\tau_{\text{op}}(\omega, T)$ and the mass enhancement (or energy renormalization) parameter $\lambda_{\text{op}}(\omega, T)$ for various bulk and 2D materials as obtained with adiabatic (A), nonadiabatic (NA), and full nonadiabatic (NA+ τ) methods. Note how the scaling of the low-frequency and low-temperature regime of $1/\tau_{\text{op}}$ is modified under the effect of NA phonon broadening.

MgB₂, 1L Gr, and 1L Gr-H. On the other hand, the NA phonon broadening and the accompanying redistribution of EPC in $\alpha^2 F(\omega)$ induce small increase of T_c in C (e.g., around 6% for $\mu^* = 0.15$). Note also a small broadening-induced increase of T_c in the case of 1L WTe₂. The latter two examples serve as an illustration on how the NA broadening effects can be quite beneficial for obtaining higher values of T_c , and it is quite possible that these dynamical corrections could be higher and more emphasized for systems with soft phonon modes [85] that are anharmonic and strongly coupled to electrons [29, 30] (e.g., charge-density-waves materials and systems at the verge of phase transition).

Having in mind the available experimental and theoretical adiabatic results, we emphasize that the NA renormalizations presented here generally improve the agreement. Namely, the theoretical first-principles estimations of T_c for MgB₂ are 50-55 K when anisotropic electron-phonon interaction and averaged Coulomb repulsion term are employed [43, 86, 87], while experimental value is $T_c = 39$ K [40] (difference of about 22-29%). As we show here by using the isotropic Allen-Dynes solution to Eliashberg equations, the substantial part of this discrepancy could be resolved by the NA effects (inducing decrease of T_c by 8-12%). Further, the *ab-initio* results of T_c for the hole-doped diamond are underestimating the experimental values [45, 47], while the present results demonstrate how the NA phonon broadening in C can enhance T_c . However, we note that the obtained increase is not enough to reproduce the experiments and that

the boron-related vibrational modes are instrumental for understanding the superconductivity in hole-doped diamond [46, 48]. Also, regardless of the doping concentration and the type of calculation, theoretical predictions of transition temperature in 1L MoS₂ ($T_c \gtrsim 4$ K) [54, 55, 59] are always much higher than experimental values, which are ~ 1 -2 K [56, 57]. Our results suggest that the dynamical renormalizations could improve this disagreement. Experimental results for WTe₂ are available as well, however, only for small electron concentrations [63, 64], where we do not expect significant NA modifications.

We would also like to point out that the previous adiabatic results of λ and T_c for all of the presented systems are in a good agreement with our adiabatic results (see Supplementary Figure 4).

Recently, dynamical effects on superconducting properties via dynamical screening of EPC matrix elements were studied by means of real-time time-dependent-density-functional theory combined with molecular dynamics [24]. The corresponding conclusion, based on the 1L Gr and 1L Gr-H cases, is that the dynamical screening that enters g^2 , e.g., via the dielectric function $\epsilon(\mathbf{q}, \omega)$, can overcome the effects of the NA frequency renormalization (hardening), and lead to the enhancement of λ and T_c compared to the static-screening calculations. These results are, however, hard to compare with the present work. On the one hand, the dynamical screening of the EPC matrix elements g is unfortunately out of reach for the present many-body perturbation approach that uses phonon self-energy within DFPT [1, 42, 88]. On

the other hand, the approach from Ref. [24] includes the dynamically-screened g and NA frequency renormalizations, but, does not account for the NA phonon broadenings. Also, it uses a frozen-phonon scheme to account for phonon dynamics and is therefore able to include only a few modes in calculations of the total λ (i.e., the $\mathbf{q} = 0$ and $\mathbf{q} = K$ optical modes for 1L Gr, and only the $\mathbf{q} = 0$ optical mode for 1L Gr-H). We stress out that the fine \mathbf{q} grids are necessary to reach the numerical convergence and account for the full NA effects of the Kohn anomalies. Also, we do not expect that the dynamical screening of EPC will play an important role in modifying the EPC properties for the materials with NA Kohn anomalies away from the Γ point, e.g., in multivalley materials such as 1L MoS₂, 1L As, and 1L WTe₂, since $\epsilon(\mathbf{q}, \omega) \approx \epsilon(\mathbf{q}, 0)$ for large \mathbf{q} [76, 89].

Figure 5 depicts the results for optical (i.e., electron-hole pair) scattering rate $1/\tau_{\text{op}}$ that enters optical conductivity formula (or current-current response tensor) and can be expressed in the following form [9, 10, 20, 26, 65, 66]

$$1/\tau_{\text{op}}(\omega, T) = \frac{\pi}{\omega} \int d\Omega \alpha^2 F(\Omega) \left[2\omega \coth \frac{\Omega}{2k_B T} - (\omega + \Omega) \coth \frac{\omega + \Omega}{2k_B T} + (\omega - \Omega) \coth \frac{\omega - \Omega}{2k_B T} \right], \quad (4)$$

having frequency ω and temperature T dependence. In addition, the results of the concomitant mass enhancement parameter (i.e., energy renormalization of electron-hole pairs) $\lambda_{\text{op}}(\omega, T)$ are shown. The latter quantity is obtained by performing Kramers-Kronig transformation of Eq. (4). Both $1/\tau_{\text{op}}$ and λ_{op} are essential in understanding the temperature dependence of optical conductivity [26], plasmon [83, 90] and phonon [83] damping (when $\omega \neq 0$), as well as for resistivity [82, 91], band renormalization [92, 93], and specific heat [26, 92] (when $\omega = 0$). Note also that the EPC constant is $\lambda = \lambda_{\text{op}}(0, 0)$.

The results show intriguing modifications of the scaling law for small- ω and small- T regime of scattering rate $1/\tau_{\text{op}}$. Namely, the NA phonon broadening effects that enter the phonon spectral function can significantly decrease the exponents x and y in $1/\tau_{\text{op}} \propto a\omega^x + bT^y$, generally, from about 3 to 2 (see Supplementary Figure 4). This NA effect is particularly emphasized for the cases where the optical phonons with large phonon linewidths are present, e.g., for MgB₂ and C. Then the large phonon linewidths extend to the low- ω part and modifies the corresponding region of $\alpha^2 F(\omega)$. The scaling change is even more pronounced for systems with low- ω acoustic modes at finite \mathbf{q} having strong NA broadening, e.g., as it is the case for 1L MoS₂ and 1L InSe. The modification of the scaling law for $1/\tau_{\text{op}}$ from the usual T^3 to T^2 that comes from the self-consistent treatment of the NA EPC was already discussed ~ 50 years ago [26, 67], but it was never thoroughly appreciated, examined and applied to the real materials. Here we confirm that the T^2 and ω^2 dependence of $1/\tau_{\text{op}}$ does not necessarily refer to the Fermi liquid result for the electron-electron scattering, but it can

equally be a fingerprint of the strong dynamical electron-phonon scattering. By combining the diagrams presented in Figs. 1(b) and 1(c), it is obvious that one can look at the present NA effects in $1/\tau_{\text{op}}$ as the effective electron-electron scatterings mediated by phonons, and thus the same phase-space arguments for the Fermi liquid result apply here. Note also the substantial modifications of $1/\tau_{\text{op}}$ at higher (i.e., linear) T that come from the large modifications of EPC λ due to NA frequency renormalizations, like in the case of 1L Gr-H and 1L InSe.

The NA effects are as well reflected in functional and intensity modifications of mass enhancement parameter $\lambda_{\text{op}}(\omega, T)$. Note for instance, that the ω and T scaling laws are also modified in λ_{op} for small ω and T when NA phonon broadening effects are accounted for. Large NA-induced modifications of λ , i.e., $\lambda_{\text{op}}(0, 0)$, are extended to finite- T region, as it is evident for 1L Gr-H and 1L InSe. This should, for example, have direct implications on the electron effective mass and its temperature dependence $m^* = m_e[1 + \lambda_{\text{op}}(0, T)]$, i.e., the band dispersion renormalizations around the Fermi level, and its microscopic *ab-initio* explanations, which are usually rooted in the adiabatic theory [68, 94–96]. Further, finite temperature $\lambda_{\text{op}}(0, T)$ [as well as $1/\tau_{\text{op}}(0, T)$], renormalized by the NA effects, which enters electron self-energy in energy-gap Eliashberg equations, can have some interesting impact on estimations of high-temperature superconductivity [97] (notice that such thermal-phonon effects are absent in McMillan’s formula for T_c).

DISCUSSION

In summary, we have thoroughly examined the influence of the NA phonon dynamics on electron-phonon properties in several theoretically and experimentally established superconductors. Contrary to the common belief, we demonstrate that the effect of “slow” electrons that lag behind the “fast” moving atoms is actually quite common and it should be considered not only for understanding the dynamics of electrons [23], but also for phonon dynamics and consequently for many physical phenomena that are founded in the electron-phonon interaction. In fact, it was recently presented in a compelling way, that nonadiabaticity is linked with the Drude weight of conduction electrons [98], which is always finite for metals and doped semiconductors. The results in Refs. [10, 19] show that the most dramatic dynamical modifications will occur when phonon-induced perturbations of conduction electron density in adiabatic and nonadiabatic regimes are disparate as well as associated with the strong EPC. See for instance Fig. 3 in Ref. [10] for the nonadiabatic perturbation of charge density in the case of MoS₂ optical out-of-plane phonon at $\mathbf{q} = 0$. Here we show that the same applies for Kohn anomalies away from the Brillouin zone center, with serious repercussions on the total EPC constant λ and superconducting properties.

We thus believe that the NA-induced modifications of EPC are quite universal and that an extension of the present NA treatment might be applicable and useful for explaining electron-phonon properties in a number of unusual and strongly-correlated materials hosting CDW, soft phonon modes or Kohn anomalies, phase transitions, superconducting phase, and enigmatic T^2 resistivity. For instance, the latter scaling law of resistivity was observed concomitantly in materials characterized with the high- T_c superconducting phase (e.g., cuprates [70]), Mott transition (e.g., SrVO₃ [73]), structural phase transition and superconductivity (e.g., SrTiO₃ [68, 69]), as well as in more conventional systems like Al [99] and TiS₂ [100]. Recently, the T^2 law was observed and discussed for novel graphene-based heterostructures, like graphene superlattice on hBN [101] and twisted bilayer graphene [102]. The superconductivity phase was discovered in the latter case, where the strongly coupled and damped optical phonons might have an important contribution to the total EPC [103, 104]. In all of these cases the corresponding interpretations were typically given in terms of the Fermi liquid theory ($1/\tau_{\text{FL}} \propto T^2$), i.e., electron-electron scattering, or some corresponding deviations. On the other hand, here we confirm Allen’s result [26] that T^2 scaling is not unique to the Fermi liquid result for the scattering rate, and it could also be a sign for the presence of the strongly damped phonons and enhanced EPC. Similar speculations were provided by Feton *et al.* [67], as well as by MacDonald [99].

Furthermore, notice that the NA corrections might be important for precise determination of transition temperature of CDW and structural phase transition [62, 105, 106], since we show that both $\mathbf{q} \approx 0$ and $\mathbf{q} > 0$ Kohn anomalies are often strongly affected by the dynamical renormalizations.

It would be interesting to examine if the NA renormalizations affect the superconducting properties in hydride systems at high pressure [107], where first-principles prediction of T_c are sometimes overestimating the experimental values [108] and some signatures of Kohn anomalies in calculated phonon spectra are present [109]. As well as for proposed few-layer and bulk derivatives of MgB₂, where superconductivity was theoretically studied [110–112].

METHODS

The ground-state *ab-initio* calculations were performed by means of the QUANTUM ESPRESSO (QE) package [79]

by applying the Perdew-Burke-Ernzerhof (PBE) functional [113] and optimized norm-conserving Vanderbilt pseudopotentials [114] with a plane-wave energy cutoff of 80 Ry. Isolated layers are described using a supercell geometry. Firstly, we perform the full relaxation in order to obtain the unit cell, and then we relax the out-of plane position of the atoms, while holding the in-plane positions fixed. Doping is simulated using a jellium model. The phonon and electron-phonon properties are extracted from the DFPT [2]. The relevant electron-phonon quantities are then interpolated by means of the Maximally-localized Wannier functions [80] and the EPW code [34]. In the latter calculations, the temperature always matches the smearing value of the ground state calculations, while the broadening in the energy-conserving delta functions is set to 40 meV or less, depending on the system. Evaluation of Eqs. (1)-(3) is done with phonon self-energy calculated within on-the-shell approximation, i.e., general excitation frequency ω in Eqs. (2) and (3) is replaced with the adiabatic phonon frequency $\omega_{\mathbf{q}\nu}$. Also, notice that the phonon self-energies in our calculations have both vertices screened, which is usual approximation but suffers from the overscreening problem [42, 88]. Nevertheless, we do not expect serious modifications to the present results, especially not in the qualitative way [42]. The Allen-Dynes version of the McMillan’s formula for T_c is calculated always with $\mu^* = 0.1 - 0.15$. Further computational details can be found in Supplementary Note 1.

ACKNOWLEDGMENTS

Useful discussions with J. Berges, S. Ponc e, and T. Wehling are gratefully acknowledged. We acknowledge financial support from the Croatian Science Foundation (Grant no. UIP-2019-04-6869) and from the European Regional Development Fund for the “Center of Excellence for Advanced Materials and Sensing Devices” (Grant No. KK.01.1.1.01.0001).

-
- [1] F. Giustino, Electron-phonon interactions from first principles, *Rev. Mod. Phys.* **89**, 015003 (2017).
 [2] S. Baroni, S. de Gironcoli, A. Dal Corso, and P. Giannozzi, Phonons and related crystal properties from density-functional perturbation theory, *Rev. Mod.*

- Phys.* **73**, 515 (2001).
 [3] A. B. Migdal, Interaction between electrons and lattice vibrations in a normal metal, *Sov. Phys. JETP* **7**, 996 (1958).

- [4] S. Engelsberg and J. R. Schrieffer, Coupled electron-phonon system, *Phys. Rev.* **131**, 993 (1963).
- [5] E. Maksimov and S. Shulga, Nonadiabatic effects in optical phonon self-energy, *Solid State Communications* **97**, 553 (1996).
- [6] F. Cerdeira and M. Cardona, Effect of carrier concentration on the raman frequencies of si and ge, *Phys. Rev. B* **5**, 1440 (1972).
- [7] E. Cappelluti, Electron-phonon effects on the raman spectrum in MgB_2 , *Phys. Rev. B* **73**, 140505 (2006).
- [8] Y. S. Ponosov and S. V. Streltsov, Raman-active E_{2g} phonon in mgB_2 : Electron-phonon interaction and anharmonicity, *Phys. Rev. B* **96**, 214503 (2017).
- [9] D. Novko, Nonadiabatic coupling effects in mgB_2 reexamined, *Physical Review B* **98**, 041112 (2018).
- [10] D. Novko, F. Caruso, C. Draxl, and E. Cappelluti, Ultrafast hot phonon dynamics in mgB_2 driven by anisotropic electron-phonon coupling, *Phys. Rev. Lett.* **124**, 077001 (2020).
- [11] E. Cappelluti, F. Caruso, and D. Novko, Properties and challenges of hot-phonon physics in metals: MgB_2 and other compounds, *Progress in Surface Science* **97**, 100664 (2022).
- [12] Y. S. Ponosov, G. A. Bolotin, C. Thomsen, and M. Cardona, Raman scattering in os: Nonadiabatic renormalization of the optical phonon self-energies, *physica status solidi (b)* **208**, 257 (1998).
- [13] Y. S. Ponosov and S. V. Streltsov, Raman evidence for nonadiabatic effects in optical phonon self-energies of transition metals, *Phys. Rev. B* **94**, 214302 (2016).
- [14] M. Lazzeri and F. Mauri, Nonadiabatic kohn anomaly in a doped graphene monolayer, *Phys. Rev. Lett.* **97**, 266407 (2006).
- [15] S. Pisana, M. Lazzeri, C. Casiraghi, K. S. Novoselov, A. K. Geim, A. C. Ferrari, and F. Mauri, Breakdown of the adiabatic born–oppenheimer approximation in graphene, *Nature Materials* **6**, 198 (2007).
- [16] S. Piscanec, M. Lazzeri, J. Robertson, A. C. Ferrari, and F. Mauri, Optical phonons in carbon nanotubes: Kohn anomalies, peierls distortions, and dynamic effects, *Phys. Rev. B* **75**, 035427 (2007).
- [17] A. M. Saitta, M. Lazzeri, M. Calandra, and F. Mauri, Giant nonadiabatic effects in layer metals: Raman spectra of intercalated graphite explained, *Phys. Rev. Lett.* **100**, 226401 (2008).
- [18] F. Caruso, M. Hoesch, P. Achatz, J. Serrano, M. Krisch, E. Bustarret, and F. Giustino, Nonadiabatic kohn anomaly in heavily boron-doped diamond, *Phys. Rev. Lett.* **119**, 017001 (2017).
- [19] T. Sohler, E. Ponomarev, M. Gibertini, H. Berger, N. Marzari, N. Ubrig, and A. F. Morpurgo, Enhanced electron-phonon interaction in multivalley materials, *Phys. Rev. X* **9**, 031019 (2019).
- [20] D. Novko, Broken adiabaticity induced by lifshitz transition in mos_2 and ws_2 single layers, *Communications Physics* **3**, 1 (2020).
- [21] P. Garcia-Goiricelaya, J. Lafuente-Bartolome, I. G. Gurtubay, and A. Eiguren, Emergence of large nonadiabatic effects induced by the electron-phonon interaction on the complex vibrational quasiparticle spectrum of doped monolayer mos_2 , *Phys. Rev. B* **101**, 054304 (2020).
- [22] P. B. Allen and J. P. Nery, Low-temperature semiconductor band-gap thermal shifts: T^4 shifts from ordinary acoustic and T^2 from piezoacoustic coupling, *Phys. Rev. B* **95**, 035211 (2017).
- [23] A. Miglio, V. Brousseau-Couture, E. Godbout, G. Antonius, Y.-H. Chan, S. G. Louie, M. Côté, M. Giantomassi, and X. Gonze, Predominance of non-adiabatic effects in zero-point renormalization of the electronic band gap, *npj Computational Materials* **6**, 167 (2020).
- [24] S.-Q. Hu, X.-B. Liu, D.-Q. Chen, C. Lian, E.-G. Wang, and S. Meng, Nonadiabatic electron-phonon coupling and its effects on superconductivity, *Phys. Rev. B* **105**, 224311 (2022).
- [25] S.-Q. Hu, D.-Q. Chen, S.-J. Zhang, X.-B. Liu, and S. Meng, Probing precise interatomic potentials by nonadiabatic nonlinear phonons, *Materials Today Physics* **27**, 100790 (2022).
- [26] P. B. Allen and R. Silbergliitt, Some effects of phonon dynamics on electron lifetime, mass renormalization, and superconducting transition temperature, *Phys. Rev. B* **9**, 4733 (1974).
- [27] F. Marsiglio, Pairing and charge-density-wave correlations in the holstein model at half-filling, *Phys. Rev. B* **42**, 2416 (1990).
- [28] B. Nosarzewski, M. Schüler, and T. P. Devereaux, Spectral properties and enhanced superconductivity in renormalized migdal-eliasberg theory, *Phys. Rev. B* **103**, 024520 (2021).
- [29] C. Setty, M. Baggioli, and A. Zaccone, Anharmonic phonon damping enhances the T_c of bcs-type superconductors, *Phys. Rev. B* **102**, 174506 (2020).
- [30] C. Setty, M. Baggioli, and A. Zaccone, Superconducting dome in ferroelectric-type materials from soft mode instability, *Phys. Rev. B* **105**, L020506 (2022).
- [31] C. Grimaldi, L. Pietronero, and S. Strässler, Nonadiabatic superconductivity: Electron-phonon interaction beyond migdal’s theorem, *Phys. Rev. Lett.* **75**, 1158 (1995).
- [32] E. Cappelluti, C. Grimaldi, L. Pietronero, and S. Strässler, Nonadiabatic channels in the superconducting pairing of fullerides, *Phys. Rev. Lett.* **85**, 4771 (2000).
- [33] L. P. Gor’kov, Superconducting transition temperature: Interacting fermi gas and phonon mechanisms in the nonadiabatic regime, *Phys. Rev. B* **93**, 054517 (2016).
- [34] S. Poncé, E. R. Margine, C. Verdi, and F. Giustino, Epw: Electron–phonon coupling, transport and superconducting properties using maximally localized wannier functions, *Computer Physics Communications* **209**, 116 (2016).
- [35] J. Nagamatsu, N. Nakagawa, T. Muranaka, Y. Zenitani, and J. Akimitsu, Superconductivity at 39k in magnesium diboride, *Nature* **410**, 63 (2001).
- [36] K.-P. Bohnen, R. Heid, and B. Renker, Phonon dispersion and electron-phonon coupling in mgB_2 and alB_2 , *Phys. Rev. Lett.* **86**, 5771 (2001).
- [37] J. Kortus, I. I. Mazin, K. D. Belashchenko, V. P. Antropov, and L. L. Boyer, Superconductivity of metallic boron in mgB_2 , *Phys. Rev. Lett.* **86**, 4656 (2001).
- [38] A. Y. Liu, I. I. Mazin, and J. Kortus, Beyond eliasberg superconductivity in mgB_2 : Anharmonicity, two-phonon scattering, and multiple gaps, *Phys. Rev. Lett.* **87**, 087005 (2001).
- [39] T. Yildirim, O. Gülseren, J. W. Lynn, C. M. Brown, T. J. Udovic, Q. Huang, N. Rogado, K. A. Regan, M. A. Hayward, J. S. Slusky, T. He, M. K. Haas, P. Khalifah,

- K. Inumaru, and R. J. Cava, Giant anharmonicity and nonlinear electron-phonon coupling in mgb_2 : A combined first-principles calculation and neutron scattering study, *Phys. Rev. Lett.* **87**, 037001 (2001).
- [40] H. J. Choi, D. Roundy, H. Sun, M. L. Cohen, and S. G. Louie, The origin of the anomalous superconducting properties of mgb_2 , *Nature* **418**, 758 (2002).
- [41] A. Eiguren and C. Ambrosch-Draxl, Wannier interpolation scheme for phonon-induced potentials: Application to bulk mgb_2 , w, and the (1×1) h-covered w(110) surface, *Phys. Rev. B* **78**, 045124 (2008).
- [42] M. Calandra, G. Profeta, and F. Mauri, Adiabatic and nonadiabatic phonon dispersion in a wannier function approach, *Phys. Rev. B* **82**, 165111 (2010).
- [43] E. R. Margine and F. Giustino, Anisotropic migdaliashberg theory using wannier functions, *Phys. Rev. B* **87**, 024505 (2013).
- [44] E. A. Ekimov, V. A. Sidorov, E. D. Bauer, N. N. Mel'nik, N. J. Curro, J. D. Thompson, and S. M. Stishov, Superconductivity in diamond, *Nature* **428**, 542 (2004).
- [45] L. Boeri, J. Kortus, and O. K. Andersen, Three-dimensional mgb_2 -type superconductivity in hole-doped diamond, *Phys. Rev. Lett.* **93**, 237002 (2004).
- [46] H. J. Xiang, Z. Li, J. Yang, J. G. Hou, and Q. Zhu, Electron-phonon coupling in a boron-doped diamond superconductor, *Phys. Rev. B* **70**, 212504 (2004).
- [47] F. Giustino, M. L. Cohen, and S. G. Louie, Electron-phonon interaction using wannier functions, *Phys. Rev. B* **76**, 165108 (2007).
- [48] F. Giustino, J. R. Yates, I. Souza, M. L. Cohen, and S. G. Louie, Electron-phonon interaction via electronic and lattice wannier functions: Superconductivity in boron-doped diamond reexamined, *Phys. Rev. Lett.* **98**, 047005 (2007).
- [49] E. R. Margine and F. Giustino, Two-gap superconductivity in heavily n -doped graphene: Ab initio migdaliashberg theory, *Phys. Rev. B* **90**, 014518 (2014).
- [50] B. M. Ludbrook, G. Levy, P. Nigge, M. Zonno, M. Schneider, D. J. Dvorak, C. N. Veenstra, S. Zhdanovich, D. Wong, P. Dosanjh, C. Strafer, A. Stöhr, S. Forti, C. R. Ast, U. Starke, and A. Damascelli, Evidence for superconductivity in li-decorated monolayer graphene, *Proceedings of the National Academy of Sciences* **112**, 11795 (2015).
- [51] S. Ichinokura, K. Sugawara, A. Takayama, T. Takahashi, and S. Hasegawa, Superconducting calcium-intercalated bilayer graphene, *ACS Nano* **10**, 2761 (2016).
- [52] G. Savini, A. C. Ferrari, and F. Giustino, First-principles prediction of doped graphene as a high-temperature electron-phonon superconductor, *Phys. Rev. Lett.* **105**, 037002 (2010).
- [53] J. T. Ye, Y. J. Zhang, R. Akashi, M. S. Bahramy, R. Arita, and Y. Iwasa, Superconducting dome in a gated-tuned band insulator, *Science* **338**, 1193 (2012).
- [54] Y. Ge and A. Y. Liu, Phonon-mediated superconductivity in electron-doped single-layer mos_2 : A first-principles prediction, *Phys. Rev. B* **87**, 241408 (2013).
- [55] M. Rösner, S. Haas, and T. O. Wehling, Phase diagram of electron-doped dichalcogenides, *Phys. Rev. B* **90**, 245105 (2014).
- [56] D. Costanzo, S. Jo, H. Berger, and A. F. Morpurgo, Gate-induced superconductivity in atomically thin mos_2 crystals, *Nature Nanotechnology* **11**, 339 (2016).
- [57] Y. Fu, E. Liu, H. Yuan, P. Tang, B. Lian, G. Xu, J. Zeng, Z. Chen, Y. Wang, W. Zhou, K. Xu, A. Gao, C. Pan, M. Wang, B. Wang, S.-C. Zhang, Y. Cui, H. Y. Hwang, and F. Miao, Gated tuned superconductivity and phonon softening in monolayer and bilayer mos_2 , *npj Quantum Materials* **2**, 52 (2017).
- [58] E. Piatti, D. De Fazio, D. Daghero, S. R. Tamalampudi, D. Yoon, A. C. Ferrari, and R. S. Gonnelli, Multi-valley superconductivity in ion-gated mos_2 layers, *Nano Letters* **18**, 4821 (2018).
- [59] P. Garcia-Goiricelaya, J. Lafuente-Bartolome, I. G. Gurtubay, and A. Eiguren, Long-living carriers in a strong electron-phonon interacting two-dimensional doped semiconductor, *Communications Physics* **2**, 81 (2019).
- [60] X. Kong, M. Gao, X.-W. Yan, Z.-Y. Lu, and T. Xiang, Superconductivity in electron-doped arsenene, *Chinese Physics B* **27**, 046301 (2018).
- [61] A. V. Lugovskoi, M. I. Katsnelson, and A. N. Rudenko, Strong electron-phonon coupling and its influence on the transport and optical properties of hole-doped single-layer inse, *Phys. Rev. Lett.* **123**, 176401 (2019).
- [62] M. Alidoosti, D. N. Esfahani, and R. Asgari, Charge density wave and superconducting phase in monolayer inse, *Phys. Rev. B* **103**, 035411 (2021).
- [63] E. Sajadi, T. Palomaki, Z. Fei, W. Zhao, P. Bement, C. Olsen, S. Luescher, X. Xu, J. A. Folk, and D. H. Cobden, Gate-induced superconductivity in a monolayer topological insulator, *Science* **362**, 922 (2018).
- [64] W. Yang, C.-J. Mo, S.-B. Fu, Y. Yang, F.-W. Zheng, X.-H. Wang, Y.-A. Liu, N. Hao, and P. Zhang, Soft-mode-phonon-mediated unconventional superconductivity in monolayer $1t' - \text{wte}_2$, *Phys. Rev. Lett.* **125**, 237006 (2020).
- [65] S. Shulga, O. Dolgov, and E. Maksimov, Electronic states and optical spectra of htsc with electron-phonon coupling, *Physica C: Superconductivity* **178**, 266 (1991).
- [66] F. Marsiglio and J. P. Carbotte, Electron-phonon superconductivity, in *Superconductivity: Conventional and Unconventional Superconductors*, edited by K. H. Bennemann and J. B. Ketterson (Springer Berlin Heidelberg, Berlin, Heidelberg, 2008) p. 73.
- [67] E. W. Fenton, J. P. Jan, A. Karlsson, and R. Singer, Ideal resistivity of bismuth-antimony alloys and the electron-electron interaction, *Phys. Rev.* **184**, 663 (1969).
- [68] D. van der Marel, J. L. M. van Mechelen, and I. I. Mazin, Common fermi-liquid origin of T^2 resistivity and superconductivity in n -type srTiO_3 , *Phys. Rev. B* **84**, 205111 (2011).
- [69] X. Lin, B. Fauqué, and K. Behnia, Scalable $\langle i \rangle t \langle /i \rangle \langle \sup \rangle 2 \langle /sup \rangle$ resistivity in a small single-component fermi surface, *Science* **349**, 945 (2015).
- [70] N. Barišić, M. K. Chan, Y. Li, G. Yu, X. Zhao, M. Dressel, A. Smontara, and M. Greven, Universal sheet resistance and revised phase diagram of the cuprate high-temperature superconductors, *Proceedings of the National Academy of Sciences* **110**, 12235 (2013).
- [71] S. Stemmer and S. J. Allen, Non-fermi liquids in oxide heterostructures, *Reports on Progress in Physics* **81**, 062502 (2018).

- [72] J. Wang, J. Wu, T. Wang, Z. Xu, J. Wu, W. Hu, Z. Ren, S. Liu, K. Behnia, and X. Lin, T-square resistivity without umklapp scattering in dilute metallic Bi_2Se_3 , *Nature Communications* **11**, 3846 (2020).
- [73] M. Mirjoleit, F. Rivadulla, P. Marsik, V. Borisov, R. Valentí, and J. Fontcuberta, Electron-phonon coupling and electron-phonon scattering in SrVO_3 , *Advanced Science* **8**, 2004207 (2021).
- [74] K. Behnia, On the origin and the amplitude of t-square resistivity in fermi liquids, *Annalen der Physik* **534**, 2100588 (2022).
- [75] A. Damascelli, Z. Hussain, and Z.-X. Shen, Angle-resolved photoemission studies of the cuprate superconductors, *Rev. Mod. Phys.* **75**, 473 (2003).
- [76] M. Düvel, M. Merboldt, J. P. Bange, H. Strauch, M. Stellbrink, K. Pierz, H. W. Schumacher, D. Momeni, D. Steil, G. S. M. Jansen, S. Steil, D. Novko, S. Mathias, and M. Reutzler, Far-from-equilibrium electron-phonon interactions in optically excited graphene, *Nano Letters* **22**, 4897 (2022).
- [77] P. B. Allen and B. Mitrović, *Theory of superconducting T_c* (Academic Press, 1983) p. 1.
- [78] P. B. Allen, Neutron spectroscopy of superconductors, *Phys. Rev. B* **6**, 2577 (1972).
- [79] P. Giannozzi and et al., Quantum espresso: a modular and open-source software project for quantum simulations of materials, *Journal of Physics: Condensed Matter* **21**, 395502 (2009).
- [80] A. A. Mostofi, J. R. Yates, Y.-S. Lee, I. Souza, D. Vanderbilt, and N. Marzari, wannier90: A tool for obtaining maximally-localised wannier functions, *Computer Physics Communications* **178**, 685 (2008).
- [81] W. L. McMillan, Transition temperature of strong-coupled superconductors, *Phys. Rev.* **167**, 331 (1968).
- [82] P. B. Allen, Electron-phonon effects in the infrared properties of metals, *Phys. Rev. B* **3**, 305 (1971).
- [83] D. Novko, Dopant-induced plasmon decay in graphene, *Nano Letters* **17**, 6991 (2017).
- [84] P. B. Allen and R. C. Dynes, Transition temperature of strong-coupled superconductors reanalyzed, *Phys. Rev. B* **12**, 905 (1975).
- [85] C. Jiang, E. Beneduce, M. Baggioli, C. Setty, and A. Zaccone, Sharp kohn-like phonon anomalies due to charge order can strongly enhance the superconducting T_c , arXiv [10.48550/ARXIV.2211.12015](https://arxiv.org/abs/10.48550/ARXIV.2211.12015) (2022).
- [86] H. J. Choi, D. Roundy, H. Sun, M. L. Cohen, and S. G. Louie, First-principles calculation of the superconducting transition in MgB_2 within the anisotropic eliashberg formalism, *Phys. Rev. B* **66**, 020513 (2002).
- [87] A. Floris, G. Profeta, N. N. Lathiotakis, M. Lüders, M. A. L. Marques, C. Franchini, E. K. U. Gross, A. Continenza, and S. Massidda, Superconducting properties of MgB_2 from first principles, *Phys. Rev. Lett.* **94**, 037004 (2005).
- [88] A. Marini, Equilibrium and out-of-equilibrium over-screening free phonon self-energy in realistic materials, arXiv [10.48550/ARXIV.2211.02573](https://arxiv.org/abs/10.48550/ARXIV.2211.02573) (2022).
- [89] C. Verdi, F. Caruso, and F. Giustino, Origin of the crossover from polarons to fermi liquids in transition metal oxides, *Nature Communications* **8**, 10.1038/ncomms15769 (2017).
- [90] I. Kupčić, General theory of intraband relaxation processes in heavily doped graphene, *Phys. Rev. B* **91**, 205428 (2015).
- [91] B. Chakraborty, W. E. Pickett, and P. B. Allen, Density of states, optical mass, and dc electrical resistance of Ta , W , Nb , and Mo using slater-koster interpolation, *Phys. Rev. B* **14**, 3227 (1976).
- [92] G. Grimvall, New aspects on the electron-phonon system at finite temperatures with an application on lead and mercury, *Physik der Kondensierten Materie* **9**, 283 (1969).
- [93] P. B. Allen and M. L. Cohen, Calculation of the temperature dependence of the electron-phonon mass enhancement, *Phys. Rev. B* **1**, 1329 (1970).
- [94] S. J. Allen, B. Jalan, S. Lee, D. G. Ouellette, G. Khalsa, J. Jaroszynski, S. Stemmer, and A. H. MacDonald, Conduction-band edge and shubnikov-de haas effect in low-electron-density SrTiO_3 , *Phys. Rev. B* **88**, 045114 (2013).
- [95] J. L. M. van Mechelen, D. van der Marel, C. Grimaldi, A. B. Kuzmenko, N. P. Armitage, N. Reyren, H. Hagemann, and I. I. Mazin, Electron-phonon interaction and charge carrier mass enhancement in SrTiO_3 , *Phys. Rev. Lett.* **100**, 226403 (2008).
- [96] M. Zacharias, M. Scheffler, and C. Carbogno, Fully anharmonic nonperturbative theory of vibronically renormalized electronic band structures, *Phys. Rev. B* **102**, 045126 (2020).
- [97] J. Appel, Role of thermal phonons in high-temperature superconductivity, *Phys. Rev. Lett.* **21**, 1164 (1968).
- [98] C. E. Dreyer, S. Coh, and M. Stengel, Nonadiabatic born effective charges in metals and the drude weight, *Phys. Rev. Lett.* **128**, 095901 (2022).
- [99] A. H. MacDonald, Electron-phonon enhancement of electron-electron scattering in Al , *Phys. Rev. Lett.* **44**, 489 (1980).
- [100] A. H. Thompson, Electron-electron scattering in TiS_2 , *Phys. Rev. Lett.* **35**, 1786 (1975).
- [101] J. R. Wallbank, R. K. Kumar, M. Holwill, Z. Wang, G. H. Auton, J. Birkbeck, A. Mishchenko, L. A. Ponomarenko, K. Watanabe, T. Taniguchi, K. S. Novoselov, I. L. Aleiner, A. K. Geim, and V. I. Fal'ko, Excess resistivity in graphene superlattices caused by umklapp electron-electron scattering, *Nature Physics* **15**, 32 (2018).
- [102] A. Jaoui, I. Das, G. D. Battista, J. Díez-Mérida, X. Lu, K. Watanabe, T. Taniguchi, H. Ishizuka, L. Levitov, and D. K. Efetov, Quantum critical behaviour in magic-angle twisted bilayer graphene, *Nature Physics* **18**, 633 (2022).
- [103] Y. W. Choi and H. J. Choi, Strong electron-phonon coupling, electron-hole asymmetry, and nonadiabaticity in magic-angle twisted bilayer graphene, *Phys. Rev. B* **98**, 241412 (2018).
- [104] Y. W. Choi and H. J. Choi, Dichotomy of electron-phonon coupling in graphene moiré flat bands, *Phys. Rev. Lett.* **127**, 167001 (2021).
- [105] M. Alidoosti, D. N. Esfahani, and R. Asgari, Superconducting properties of doped blue phosphorene: effects of non-adiabatic approach, *2D Materials* **9**, 045029 (2022).
- [106] D. Novko, Z. Torbatian, and I. Lončarić, Electron correlations rule phonon-driven instability in single layer TiSe_2 , arXiv [10.48550/ARXIV.2203.10658](https://arxiv.org/abs/10.48550/ARXIV.2203.10658) (2022).
- [107] J. A. Flores-Livas, L. Boeri, A. Sanna, G. Profeta, R. Arita, and M. Eremets, A perspective on conventional high-temperature superconductors at high pressure: Methods and materials, *Physics Reports* **856**, 1 (2020).

- [108] I. Errea, M. Calandra, C. J. Pickard, J. R. Nelson, R. J. Needs, Y. Li, H. Liu, Y. Zhang, Y. Ma, and F. Mauri, Quantum hydrogen-bond symmetrization in the superconducting hydrogen sulfide system, *Nature* **532**, 81 (2016).
- [109] I. Errea, M. Calandra, C. J. Pickard, J. Nelson, R. J. Needs, Y. Li, H. Liu, Y. Zhang, Y. Ma, and F. Mauri, High-pressure hydrogen sulfide from first principles: A strongly anharmonic phonon-mediated superconductor, *Phys. Rev. Lett.* **114**, 157004 (2015).
- [110] J. Bekaert, M. Petrov, A. Aperis, P. M. Oppeneer, and M. V. Milošević, Hydrogen-induced high-temperature superconductivity in two-dimensional materials: The example of hydrogenated monolayer mgb_2 , *Phys. Rev. Lett.* **123**, 077001 (2019).
- [111] S. Singh, A. H. Romero, J. D. Mella, V. Ereameev, E. Muñoz, A. N. Alexandrova, K. M. Rabe, D. Vanderbilt, and F. Muñoz, High-temperature phonon-mediated superconductivity in monolayer $\text{mg}_2\text{b}_4\text{c}_2$, *npj Quantum Materials* **7**, 37 (2022).
- [112] Z. Yu, T. Bo, B. Liu, Z. Fu, H. Wang, S. Xu, T. Xia, S. Li, S. Meng, and M. Liu, Superconductive materials with mgb_2 -like structures from data-driven screening, *Phys. Rev. B* **105**, 214517 (2022).
- [113] J. P. Perdew, K. Burke, and M. Ernzerhof, Generalized gradient approximation made simple, *Phys. Rev. Lett.* **77**, 3865 (1996).
- [114] D. R. Hamann, Optimized norm-conserving vanderbilt pseudopotentials, *Phys. Rev. B* **88**, 085117 (2013).